Dynamics of quasistatic directional crack growth

O. Ronsin and B. Perrin
Laboratoire de Physique de la Matière Condensée, Ecole Normale Supérieure, 24 rue Lhomond, 75231 Paris Cedex 05, France
(Received 2 May 1997)

We report extended experimental results on the dynamics of quasistatic directional crack growth in a brittle material. Straight propagation, characterized by both the propagation threshold and the crack tip equilibrium position, enables, within the Griffith energy balance framework, the extraction of the fracture energy and its dependencies with temperature and crack velocity. It is shown that the apparent variations of the fracture energy with crack velocity are an effect of the local temperature at the crack tip, which controls the relative humidity. The oscillating instability of the propagation is described and the results are compared with recent theoretical work, showing that the sensitivity to details of the experimental conditions implies special care for quantitative comparison. [S1063-651X(98)02102-3]

PACS number(s): 46.30.Nz, 62.20.Mk

I. INTRODUCTION

The study of crack growth has recently been subject to a renewal of interest among physicists. This is essentially due to the nonlinear properties of this moving boundaries problem, which the various tools developed to study dynamical systems may help one to understand. Recent studies of crack growth systems have focused on the formation of patterns, either by fragmentation [1], dessication [2], or crack interaction [3,4], and the dynamical instabilities observed during crack propagation. This last point has received much attention, both from experimental [5–8] and theoretical [9–13] points of view. Though the nature of some instabilities has been described, their mechanisms are not yet well understood.

Recent experiments [6,7] have shown, because of the localization of the growth front (the crack tip) as in directional solidification, the ability to control the propagation over a wide range of quasistatic velocities. In this paper, we present results on the dynamics of a single crack in a directional growth experiment, extending previous work [7].

After describing the experimental setup, we will show in Sec. II that this system exhibits various propagation states, depending on the amount of elastic energy stored in the samples, which enables the experimental investigation of fundamental problems in brittle fracture, while controlling the crack front velocity. Among these states, we will focus in Sec. III on straight propagation, by studying both the propagation threshold and the equilibrium crack tip position during propagation. Confrontation with an elastic model gives access to the fracture energy of glass, as well as its dependencies with the control parameters of the experiment. We will then assess in Sec. IV the problem of the stability of straight crack, and using the results obtained on the fracture energy, we will quantitatively confront our experimental data with models of quasistatic crack stability.

II. PROPAGATION STATES

The experiment is analogous to directional crystal growth: a crack front is spatially localized within a thermal gradient, and propagation is achieved by driving hot glass samples into a cold bath at constant velocity V (Fig. 1). The samples are thin soda-lime glass plates of thickness e less than a millimeter, length of about 1 m, and width L between 3 and 40 mm. The plates are driven through two temperature baths: they first pass through an oven at temperature $T_0+\Delta T$, made of two parallel heating elements, separated by a 1.1 mm gap to enable the translation of the glass plate without friction while ensuring good thermalization; then the plates dip into a large basin of about 30 liters of water at ambient temperature T_0. A circulation of water maintains a constant level of the surface and increases the efficiency of the cooling of the plate. The dynamic meniscus present at the contact between the glass and the water is controlled by preparation of the glass surfaces with a hydrophobic solution [14], which imposes a roughly constant contact angle of 90°. These precautions enable a control over the distance h between the heater and the cooling bath to within 0.5 mm, for values between 5 and 10 mm. The driving of the glass plates at constant velocity V is ensured by a stepping motor, paced by a TTL clock signal, within the range 0.01 to 10 mm s^{-1}.

The stationary thermal field thus induced inside the glass

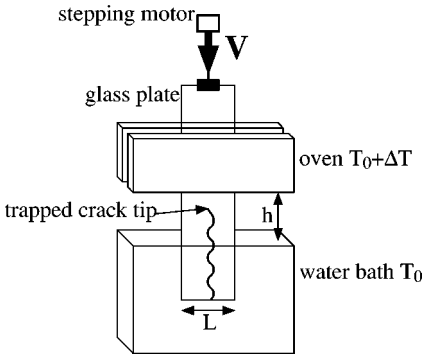

FIG. 1. Schematic setup of the directional crack growth experiment: a thin glass plate of thickness $e=0.9$ mm and width L is driven at constant velocity V from a heater (temperature $T_0+\Delta T$), into a water bath (temperature T_0), at a distance $h=5$ mm lower. The resulting thermal field induces stress in the plate that can trap the crack tip in the region between the two temperature baths. Then, as the plate moves within the thermal field, the crack front grows through the glass at the controlled velocity V.

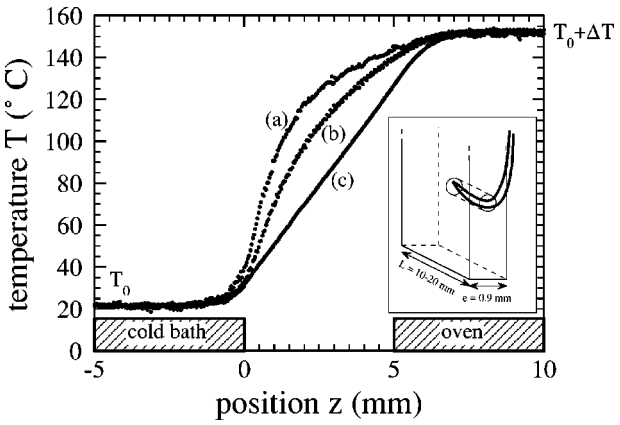

FIG. 2. *In situ* measurement of the thermal field is achieved with a type T thermocouple, made of 0.05 mm diameter wires, and inserted inside a hole drilled on the side of a 0.9 mm thick glass plate (inset). The plate is driven through the temperature baths at constant velocity V, and the temperature is recorded as a function of time, giving the spatial distribution of the temperature inside the glass plate, here plotted for three different values of the driving velocity V. We clearly see the two distinct regimes, of pure diffusion at low velocities [$V=0.05$ mm s^{-1} (a)], and advection at higher velocities [$V=0.3$ (b), and 0.5 mm s^{-1} (c)].

samples depends on the difference of temperature ΔT, the distance h between the baths, and on the driving velocity V, which advects the temperature field from the heater towards the cold bath and concentrates the thermal gradient above the water level, over a characteristic distance $d_{\mathrm{th}}=D/V$, where D is the thermal diffusion coefficient of the glass ($D\simeq 0.5$ mm^2 s^{-1}). We have measured the temperature field inside the glass plates by inserting a type T thermocouple, made with 0.05 mm diameter wires, inside a hole 5 mm deep with a 0.3 mm diameter drilled on the side of a 0.9 mm thick glass plate (inset of Fig. 2). Driving this plate within the baths at constant velocity V, and recording the temperature as a function of time t, gives the spatial longitudinal thermal field $T(z=z_0-Vt)$ inside the plate. The initial position z_0 of the thermocouple was chosen high enough within the hot bath for the thermal field to be in a stationary state when the probe approaches the gap h. Figure 2 presents the measured temperature fields for different values of the driving velocity V. Within the region between the baths, we recover the expected variations of the temperature field as a function of V: at low velocities, the advection is negligible and the thermal gradient is uniform, but at higher velocities, we observe the manifestation of advection through the localization of the thermal gradient near the cold bath, and the higher the velocity, the stronger the effect. Let us note, however, that the temperature baths are imperfect, as the transitions between the three zones, the hot thermostat, the gap h, and the cold thermostat occur over a distance of order 1 mm. These measurements are reproducible, and for fixed values of V and h, the temperature profile scales with the temperature difference ΔT. This temperature measurement setup also enabled us to check that the stationary temperature field is effectively reached after a characteristic time $\tau\simeq h^2/D\simeq 50$ s. The glass samples thus need to be translated over a distance $d\simeq V\tau$ in order to reach the stationary state of the temperature field.

The thermal stress field in the interior of the glass plate is

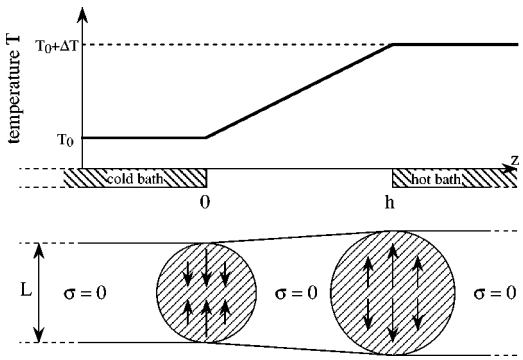

FIG. 3. In an elastic plate free to deform, a uniform gradient does not induce stress. The stress only comes from the variations of the gradient (here at $z=0$ and $z=h$), and extend over a region of characteristic size, the width L of the plate.

induced by the thermal expansion of the glass. Here, the plate's edges are free to deform, and a uniform temperature gradient leads to no stress [15], only gradient variations; i.e., the second spatial derivatives of the thermal field induce stress inside the plate. For example, in the case of a pure diffusive thermal field ($V=0$), the stress comes from the boundaries ($z=0$ and $z=h$) between the three regions of uniform gradient (Fig. 3), but an assumption of perfect thermal baths then leads to a discontinuity of the gradient, which overestimates the stress field [7]. According to the Saint-Venant principle [15], the stress field induced by these gradient variations will extend over a characteristic distance of the order of the plate's width L. This parameter L thus enables the control of the amount of elastic energy stored inside the plate.

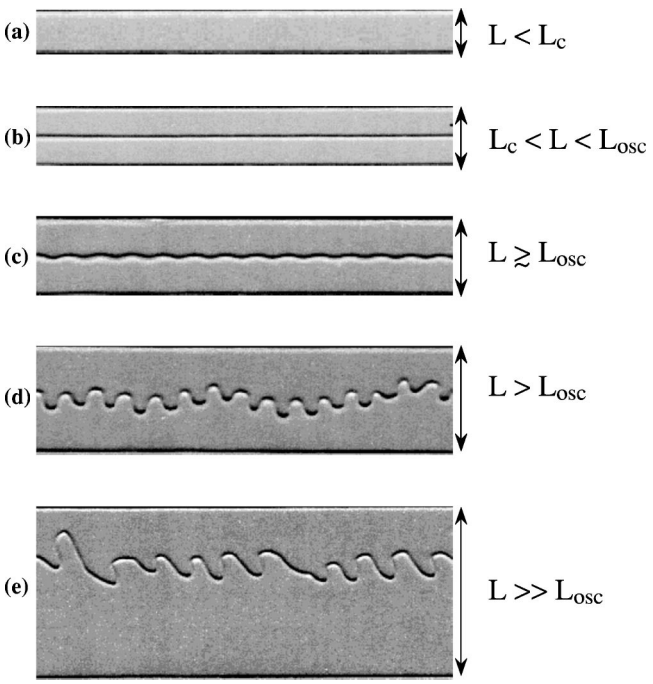

FIG. 4. The various propagation states in the directional crack growth experiment. According to the plate's width L, which controls the amount of elastic energy available, three states are observed, no propagation for $L<L_c$ (a), straight propagation for $L_c<L<L_{\mathrm{osc}}$ (b), and oscillating propagation for $L>L_{\mathrm{osc}}$ (c). Further increase of L leads to irregular behavior of the crack (d) and (e).

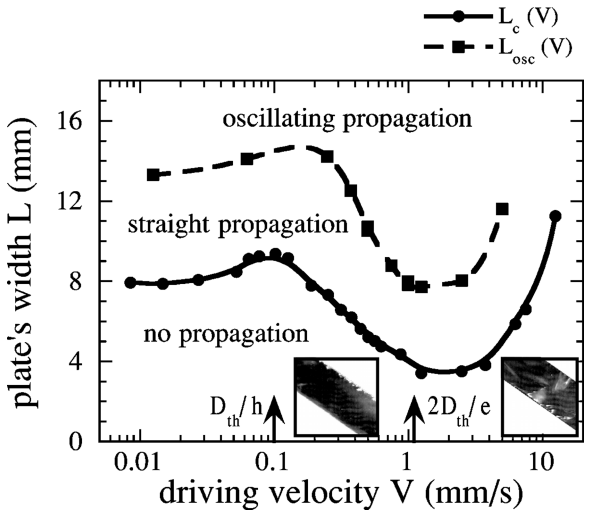

FIG. 5. As a function of the driving velocity V, the bifurcation curves $L_c(V)$ and $L_{\mathrm{osc}}(V)$ reflect the variations of the thermal field with V: they are controlled by the distance h between the baths at low velocities, the thermal length d_{th} in their decreasing part, and the thickness e of the plate at higher velocities, leading to a three-dimensional problem. The crack surfaces shown in the inset illustrate well this transition from two-dimensional to three-dimensional fracture process.

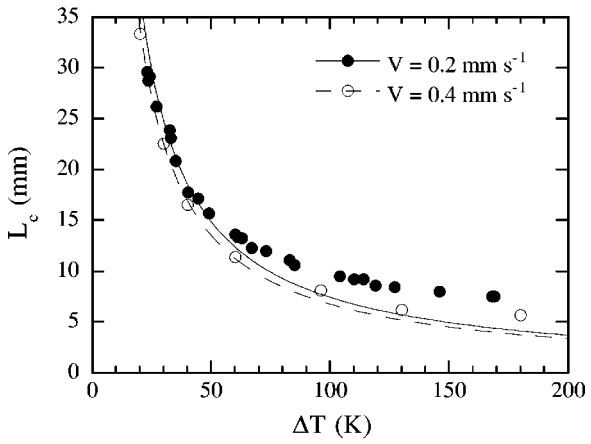

FIG. 6. Variations of the propagation threshold L_c as a function of the temperature difference ΔT between the baths, for two fixed driving velocities $V=0.2$ mm s^{-1} (●) and $V=0.4$ mm s^{-1} (○). The lines correspond to the best fit of these data to a $1/\Delta T$ scaling, which is better at higher velocities, the discrepancy being attributed to the finite extension of the stress sources.

Crack nucleation often requires much more energy than its propagation, as it occurs essentially from microscopic surface defects [16,17], which have a lower stress concentration factor than a propagating crack tip, because of their small size. The creation of a new crack will thus depend on the surface state of the glass plate, which is difficult to control. The glass plates are therefore seeded by scratching the leading edge, and the elastic energy is only used for crack propagation.

In a given thermal field (ΔT, h and V fixed), the growth state depends on the plate's width L [7]: for low values of the width, the crack does not grow [Fig. 4(a)]; when L is greater than a critical value L_c, the crack grows straight, cutting the plate in two equal parts [Fig. 4(b)]. This straight propagation is stable as long as the plate's width remains below a second critical value L_{osc}, above which the crack path becomes wavy, making regular oscillations near the instability threshold [Fig. 4(c)]. Regular oscillations become less and less regular as L is further increased [Figs. 4(d) and 4(e)]. These propagation states were always observed, whatever the thermal field (i.e., ΔT, V, and h). A phase diagram can thus be drawn in the parameter space (L,V), with the width L controlling the available elastic energy, and the driving velocity V controlling both the longitudinal crack velocity (which is the absolute velocity for straight propagation) and the advection of the thermal field.

Let us recall the main result concerning the propagation states, obtained in Ref. [7]. A typical phase diagram is plotted in Fig. 5 in semilogorithmic scale, showing the three states of propagation with the transition lines, $L_c(V)$ separating the no-propagation state from straight propagation, and $L_{\mathrm{osc}}(V)$ separating the straight from the wavy propagation. These two curves are roughly parallel and clearly show three different regimes as a function of the driving speed V. These regimes have been related [7] to the variations of the stationary thermal field with V. The low velocity regime corresponds to a pure diffusive, velocity independent field, when the thermal length d_{th} is greater than the distance h between the baths. At higher velocities, the advection process results in the decrease of the critical widths with V, and lasts as long as d_{th} remains bigger than the half thickness $e/2$ of the glass plate, for which the temperature is no longer homogeneous inside the plate, leading to increasing critical widths with V. This last transition from a two-dimensional to a three-dimensional process is clearly visible on the crack surfaces, which are smooth at low velocities and rough at high velocities (inset of Fig. 5). The following analysis will be restricted to the two first two-dimensional regimes.

III. STRAIGHT CRACK PROPAGATION

The energetic difficulty of crack nucleation implies that the curve $L_c(V)$ (Fig. 5) only reflects the transition from the propagating state to the nonpropagating one. The critical width L_c is thus measured by using plates of slowly decreasing width. Starting with a width $L>L_c$, the seeded crack first propagates through the plate at the constant driving velocity V, and stops when $L=L_c$, its tip sinking with the plate into the water bath. The rate of width variation is chosen to be less than 1% so that the error on the steady temperature field matches the width within 1%. In such conditions, the measurement of the critical width L_c is reproducible with less than 5% dispersion.

Another interesting dependence of L_c is its variations with the temperature difference ΔT at fixed driving velocity V. In Fig. 6, we show such a dependence for two fixed values of the driving velocity inside the advective regime of the temperature field ($V=0.2$ and $V=0.4$ mm s^{-1}). L_c decreases with ΔT, showing the increase in elastic energy density with ΔT, so that for larger values of ΔT, less width is needed for crack propagation. The figure also shows the best fit of these data with the scaling $L_c \propto 1/\Delta T$, which is better at high velocities. This scaling can be written $L_c^2(\Delta T)^2=\mathrm{const}$, corresponding to onset of propagation when the elastic energy

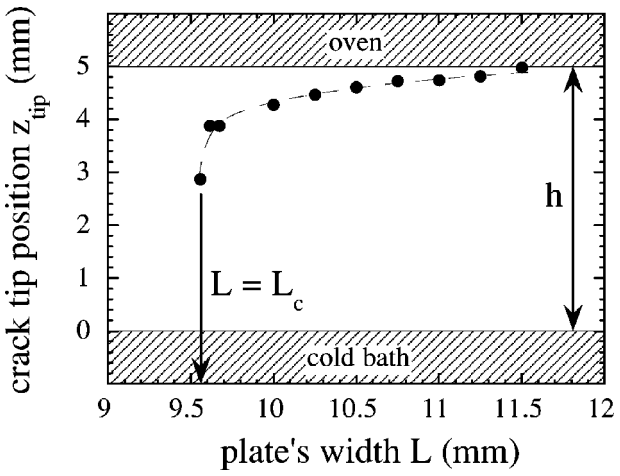

FIG. 7. Evolution of the equilibrium crack tip position z_{tip} as a function of the plate's width L for fixed values of the driving velocity $V=0.125$ mm s^{-1}, temperature difference $\Delta T=135°$C, and the distance $h=5$ mm between the temperature baths. The crack tip matches its position toward the high stress region near the cold bath to compensate the decrease in plate's width L when approaching the propagation threshold ($L\rightarrow L_c$).

([volume $\propto L_c^2$]$\times$[energy density $\propto(\Delta T)^2$]) released by crack propagation reaches a threshold level, as stated by the Griffith criterion for crack growth [16]. The discrepancy between this scaling and the experimental observation can be attributed to the finite extension of the stress sources (the temperature gradient variations), which decreases with velocity and results in a lower effective affected volume, whose effect is stronger at low values of L_c.

This threshold L_c is clearly linked to the minimal amount of energy required for crack propagation. For larger width, i.e., inside the straight propagation region $L_c<L<L_{\mathrm{osc}}$, the system adapts to the excess of available elastic energy through another parameter: the crack tip position z_{tip}.

Direct *in situ* images of the crack tip are obtained using a video camera, with a spatial resolution of 0.1 mm and a time sampling between images of 1/50 s. This is only possible when the equilibrium position lies between the temperature baths, where reflection of light on the crack surface enables the visualization of the crack tip.

We have measured the tip equilibrium position z_{tip} when traveling through the (L,V) phase diagram. The matching of the system to the available elastic energy via the crack tip position is clearly illustrated in Fig. 7, where we have studied the equilibrium tip position z_{tip} as a function of the plate's width L ($>L_c$) for a fixed temperature field (ΔT, h, and V fixed). For $L>L_c$, the available elastic energy is greater than what is needed for propagation, the crack tip position stabilizes near the hot bath, i.e., in a lower stressed region. As the width L decreases toward L_c, the available energy decreases, and the tip position goes closer to the cold bath, in a higher stressed region. Finally, when L reaches its critical value L_c, the propagation stops and the tip falls with the plate into the cold bath.

For fixed values of the plate's width L above its critical value L_c, the crack tip position depends on the driving velocity V and approximately follows the evolution of the thermal field with V.

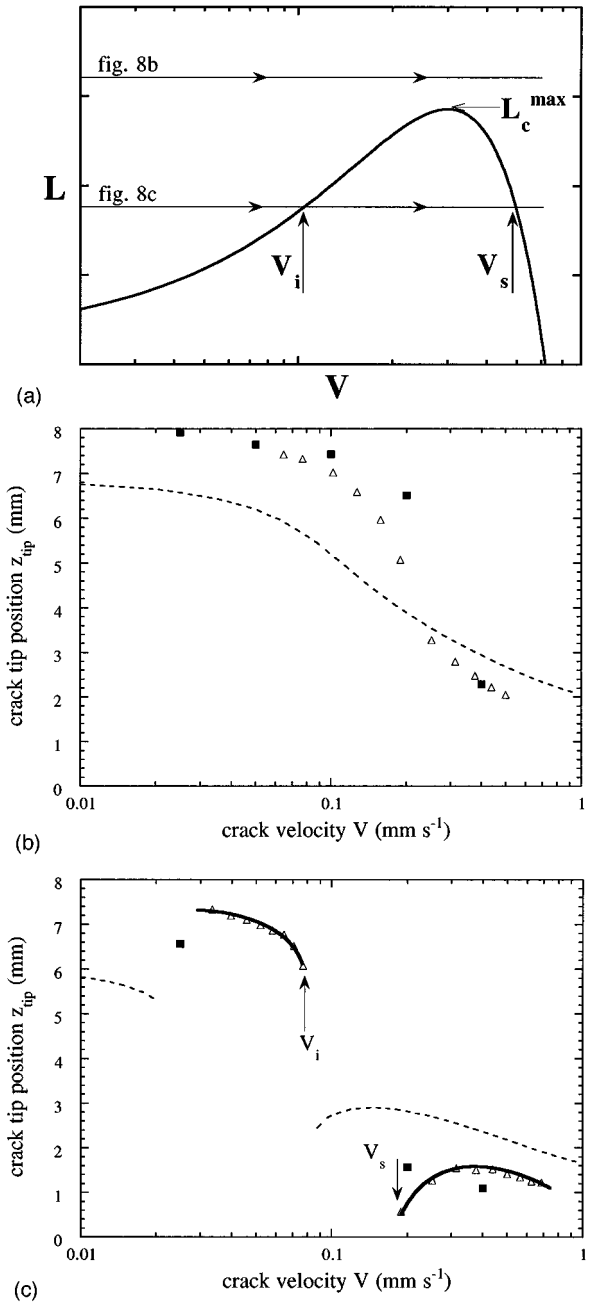

FIG. 8. Evolution of the measured equilibrium crack tip position z_{tip} with respect to the driving velocity V for two different values of the plate's width L (triangles), with $\Delta T=135$ °C, and $h=7.5$ mm. When L is higher than the propagation threshold L_c in the whole range of velocities ($L>L_{\mathrm{max}}$), the tip position continuously decreases with V, following the advection of the thermal field towards the cold bath (b). Smaller values of L can place the system in different propagation states depending on V (c). Approaching the non-propagation region $[V_i,V_s]$, the crack tip goes closer to the cold bath, but recovers the general trend far from it, the thick lines are guides for the eye. (b) and (c) also show the predicted crack tip positions, first with an ideal thermal field (dashed lines), and with the measured one (squares).

Let us note that the $L_c(V)$ curve presents a maximum L_c^{max} [see Fig. 5 and Fig. 8(a)]. For $L>L_c^{\mathrm{max}}$, the equilibrium position of the crack tip above the cold bath is observed to be a continuously decreasing function of the velocity [Fig.

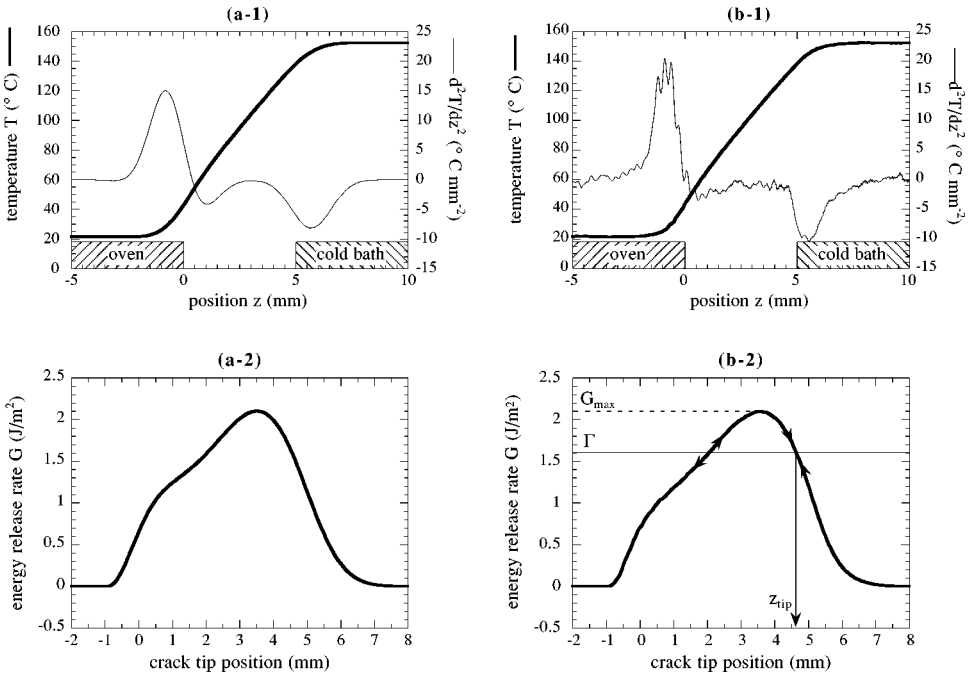

FIG. 9. The use, in the model, of the measured thermal field, either directly (a) or by fitting it with analytical functions (b), leads to similar quantitative results for the energy release rate $G(z)$ as a function of the crack tip position z. The Griffith energy balance directly gives the stable equilibrium tip position z_{tip} by the intersection of the energy release rate $G(z)$ and the fracture energy Γ.

8(b)], and illustrates the advection of the thermal field towards the cold bath. For $L_c(V=0)<L<L_c^{\max}$ [Fig. 8(c)], the crack cannot propagate in a given range of $V(V_i<V<V_s)$. Approaching $V_i(V_s)$ from low (high) velocity, the equilibrium position of the crack tip z_{tip} is markedly decreasing: the tip sinks and ''dies'' into water when entering the nonpropagating region.

We can analyze these results within the Griffith energy balance framework [16]: the crack tip is at an equilibrium position when the amount of elastic energy released for a crack growth of a unit length equals the amount of energy needed to create the corresponding surfaces. Per unit surface, this equilibrium can be written as

$$G(z_{\mathrm{tip}})=2\gamma, \tag{1}$$

where γ is the surface energy of the fractured material, and G is the amount of elastic energy released by the creation, during crack growth, of a unit surface. G is the energy release rate, and only depends, apart from the elastic properties of the material, on the sample geometry (width L and crack tip position z_{tip}), and the loading conditions (thermal field). A usual extension of this equation, in order to account for dissipation processes other than pure surface energy, consists in introducing the fracture energy Γ, which contains the surface energy 2γ and other *a priori* unknown terms, such as plastic dissipation, chemical effects, etc. [17] Equation (1) is then

$$G(z_{\mathrm{tip}})=\Gamma. \tag{2}$$

Using linear elastic fracture mechanics, one can calculate the energy release rate G as a function of the straight crack tip position z within the thermal field. This has been performed, under plane stress conditions, in Ref. [10] for an infinite strip of width L, containing a semi-infinite static crack, submitted to a thermal field $T(z)$. These conditions apply as long as the thermal field is homogeneous inside the plate, that is, as long as the driving velocity V is lower than its limiting value $V=2D/e$ (cf. Sec. II). At such velocities, of order 1 mm s^{-1}, much lower than the sound speed in glass (hundreds of meters per second), the crack growth is in quasistatic conditions, and the effect of the driving velocity V only accounts via the thermal profile $T(z)$. Recall that the stress comes from the second spatial derivative of the profile, therefore quantitative comparison with the experimental results requires special care in the determination of the profile. We use the measured thermal field in order to make the computed energy release rate match most precisely the experimental conditions. To include this thermal profile into the elastic stress computation, two distinct methods have been used. First the measured profile was fitted with an analytical function. To account for the finite extension of the transitions between the three distinct regions of the temperature field [Fig. 9(a)], we chose the second derivative of the fitting function to be a sum of two or three Gaussians, whose parameters were adjusted so that the function fits the measured thermal field. In the second method, we directly used the measured thermal field. The high frequency noisy measured signal has large local second derivatives, but each of these induces stress over a spatial length of the order of the plate's width. The Saint-Venant principle thus acts as a low-pass filter, with a characteristic size, the width L of the plate [Fig. 9(b)]. Furthermore, the sampling step of the spatial thermal field measurement was chosen small enough for the numeric calculation, performed with the use of fast Fourier transforms [10], to provide good accuracy. The similarity of the energy release rate functions $G(z)$, obtained with both methods, is presented in Fig. 9 [(a-2) and (b-2)], showing that they both are relevant. Because it is more straightforward and requires less computation time, we essentially used the second method to obtain the energy release rate from a measured thermal profile.

The propagation state of a straight crack in the plate is given by the comparison between the energy release rate and the fracture energy. Depending on the maximum value $G_{\max}$ of $G(z)$, there can be either none, one, or two intersections

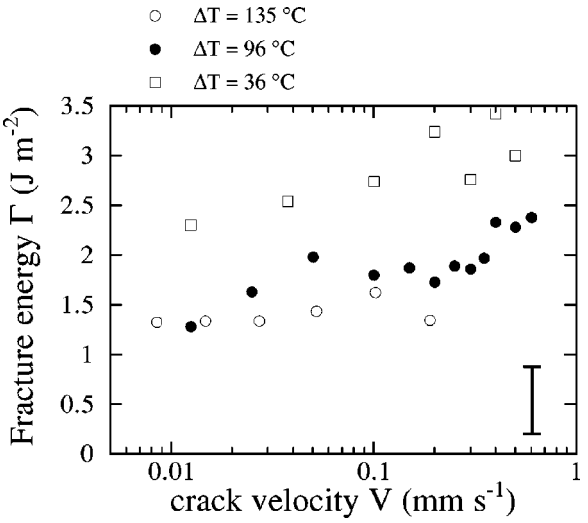

FIG. 10. Measured fracture energy Γ as a function of the crack velocity V for three different values of ΔT [135 (○), 96 (●), and 36 °C (□)], showing a clear dependence with ΔT. The error bar is in the lower right corner.

between $G(z)$ and the fracture energy Γ [Fig. 9(b-2)]. The maximum $G_{\max}$ scales as $(\Delta T)^2$, but has no simple dependence with L, though, as expected by applying the Saint-Venant principle, it increases with the plate width L, showing that for low enough values of L, there is no intersection, and thus no propagation. Additionally, for large values of L, there are two solutions for the equation $G(z)=\Gamma$, corresponding to two possible equilibrium positions for the crack tip, though only the solution in the decreasing part of $G(z)$ at $z=z_{\text{tip}}$ is stable. As the plate is translated at constant velocity V through the thermal field, the crack propagates inside the plate. The propagation threshold L_c corresponds to merging the two intersections into one, at which point $G_{\max}=\Gamma$.

Adjusting the fracture energy on the measured propagation threshold at low velocities, this model has shown to be in good qualitative agreement with the whole dependence of L_c with V [7], even with an ideal thermal field, only controlled with the two characteristic lengths, the distance h between the temperature baths at low velocities, and the thermal diffusion length d_{th} at high velocities.

Quantitative comparison can only be achieved by extracting the unknown fracture energy Γ, the only adjustable parameter of the model, the energy release rate being calculated with the measured thermal field. It was shown in Ref. [7] that for high values of ΔT, the so derived fracture energy had a weak dependence with the velocity V within experimental precision.

For a better characterization of this result, we have studied the dependence of the fracture energy Γ with the temperature difference to account for lower values of ΔT. Figure 10 shows the fracture energy Γ as a function of the crack velocity V for three values of the temperature difference ΔT. The velocity dependence is not so clear (especially within the experimental precision), but we can see a clear decrease of Γ with ΔT.

These apparent variations of the fracture energy with V and ΔT can be expressed as a dependence with a single parameter, the local temperature T_{tip} of the glass at the crack tip. As the fracture energy was measured as the maximum

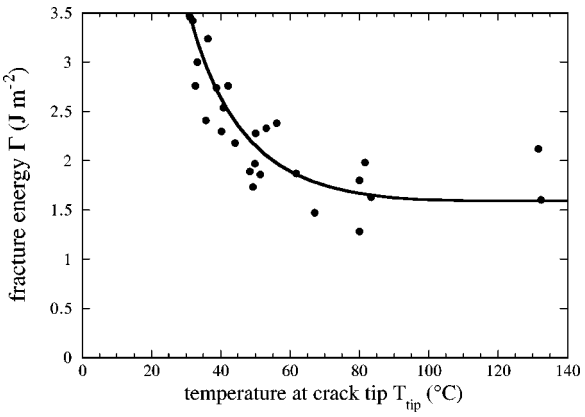

FIG. 11. The measured fracture energy Γ plotted as a function of local temperature T_{tip} at the crack tip for various values of V (0.01–1 mm s^{-1}) and ΔT (20 to 180 °C) shows a unique dependence that can be related to stress corrosion effects (the solid curve is a guide for the eye).

$G_{\max}$ of the energy release rate $G(z)$ at the propagation threshold L_c, we can thus obtain the position z_{tip} of this maximum, which is the crack tip position at the propagation threshold. The temperature field $T(z)$ inside the plate being known, we can obtain the local temperature in the plate at this position $T_{\text{tip}}=T(z_{\text{tip}})$.

Figure 11 shows the dependence of the fracture energy Γ with this temperature T_{tip}, for fracture energies measured both at various ΔT and crack velocities V. They all group on the same curve, indicating that variations with both ΔT and V are due to the dependence on T_{tip}. A decrease of Γ with T_{tip}, with a saturation at high temperatures, is clearly observed.

This dependence of the fracture energy on the local temperature at the crack tip is probably related to the well-known effects of water on crack propagation [18]. Water molecules are known to chemically react with the highly stressed Si-O-Si bonds of the glass at the crack tip, which results in a diminution of the fracture energy with the relative humidity. We expect the pressure of water vapor at the crack tip to increase with the local temperature at the crack tip, with a saturation at high temperatures, and thus to apparently depend on ΔT and V, as they both modify the equilibrium tip position within the thermal field. It should be noted through, that the link between the local temperature and the relative humidity at the crack tip is not clear. Furthermore, direct comparison with classical fracture experiments under controlled environment is not straightforward as such experi-

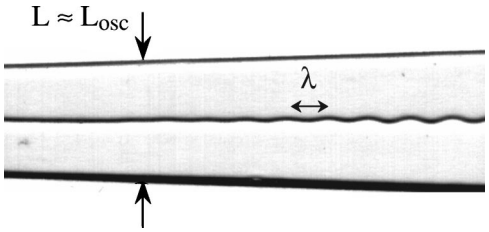

FIG. 12. Scanned image of a glass sample showing the progressive transition from straight to oscillating propagation as a function of the plate's width L. The glass plate has here a high relative increase in width for demonstrative purposes.

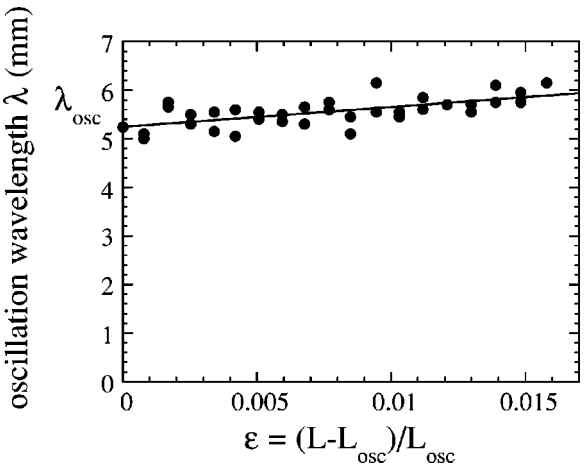

FIG. 13. Oscillation wavelength λ as a function of the relative distance to the instability threshold $\epsilon=(L-L_{\rm osc})/L_{\rm osc}$, for $\Delta T=135$ °C, $h=5$ mm and $V=0.2$ mm s^{-1}, showing the finite value of the wavelength $\lambda_{\rm osc}$ at the threshold and the low dependence with ϵ.

ments usually measure the velocity response to an increase in energy release rate and here, we impose the stationary crack velocity V and extract the fracture energy at a stable equilibrium position of the crack tip.

We have checked these measurements of the fracture energy Γ from the equilibrium crack tip positions. Above the propagation threshold L_c, the evolution of the crack tip position $z_{\rm tip}$ with V is qualitatively well reproduced by the elastic model, as shown in Figs. 8(b) and 8(c), but the quantitative discrepancy is high. Using both the fracture energy extracted from the propagation thresholds L_c and the measured thermal field, the predicted crack tip positions come closer to the measured ones [Figs. 8(b) and 8(c)], though there still remains a large uncertainty, mainly due to the error caused by the high slope of the energy release rate $G(z)$ around the equilibrium position $z_{\rm tip}$, inside the straight propagation state.

IV. OSCILLATING INSTABILITY

Straight crack propagation remains stable as long as the plate's width remains below the critical value $L_{\rm osc}$. For plates larger than this threshold, the crack path is no longer straight. Near the threshold $L_{\rm osc}$, the crack grows, forming regular oscillations with a well-defined wavelength λ. As the width L is increased further, these oscillations become less and less regular [Fig. 4(c)]. One can eventually observe, in these last regimes, the nucleation of a new crack from the crack surface where the curvature is high, thus forming a stress concentrator.

The oscillation threshold $L_{\rm osc}(V)$ is measured, as for the propagation threshold, by slowly varying the plate's width L (Fig. 12). This can be achieved either by an increase or a decrease of L, as there is, here, no nucleation problem. The rate of variation of the width L is chosen as for the measurement of L_c, i.e., lower than 1%. The measurement of $L_{\rm osc}$ consists in the determination of the point at which the path followed by the crack is not straight but oscillating, and is thus procedure dependent. This has been achieved by various methods, by touching the cracked surfaces, or by sight in razing incidence, leading to the localization of the threshold within a region of about 1 cm along the crack path. With such a procedure, we found no significant difference in $L_{\rm osc}$ measured with either increasing or decreasing plate's widths.

The other characteristic quantity of this instability is its oscillation wavelength λ. Figure 12 shows a numerized (scanned) image of a cracked glass plate, which shows the progressive transition from straight to oscillating propagation. Following the path, we can draw the evolution of the wavelength λ as a function of the relative distance to the instability threshold $\epsilon=(L-L_{\rm osc})/L_{\rm osc}$, as shown in Fig. 13. The wavelength has a finite value $\lambda_{\rm osc}$ at the threshold and slowly increases with the plate's width $L\geqslant L_{\rm osc}$.

To determine the nature of this instability, we have studied the spatiotemporal dynamics of the crack tip, and measured by video means both its longitudinal and transversal positions as a function of time just above the onset (Fig. 14): the instability only consists in a transversal oscillation of the crack tip and the longitudinal propagation speed remains, as in the straight regime, the driving velocity V. The oscillation frequency f is thus linked to the wavelength measured along the path by $\lambda=V/f$, and checked the result obtained by direct measurement.

The variation of the two characteristic quantities $L_{\rm osc}$ and

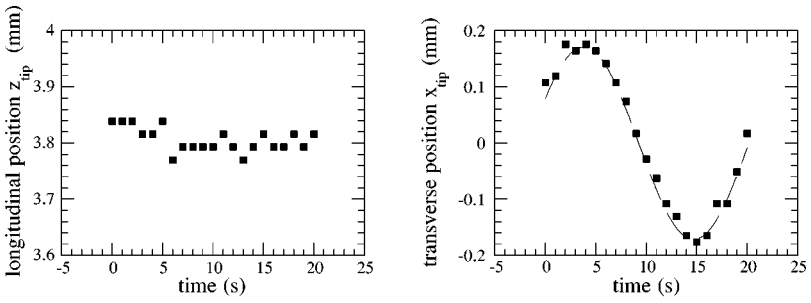

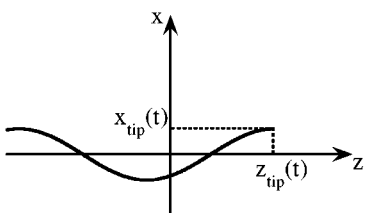

FIG. 14. The time evolution of both longitudinal and transversal crack tip positions just above the onset of the oscillating instability shows that the instability only consists in a transversal oscillation of the crack tip.

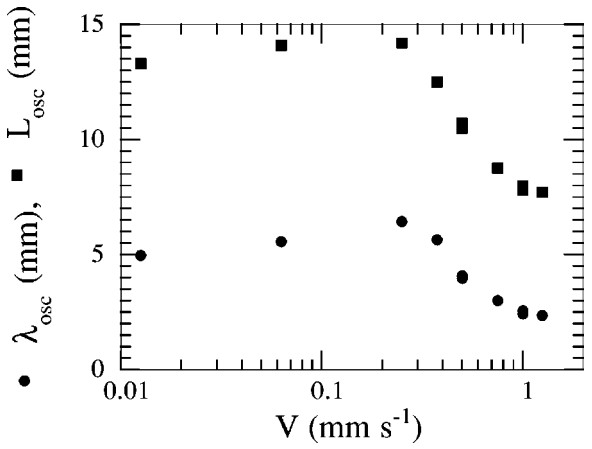

FIG. 15. Variations of L_{osc} and λ_{osc} with the driving velocity V for $\Delta T = 135\,^{\circ}\mathrm{C}$ and $h = 5$ mm, showing their similar behavior.

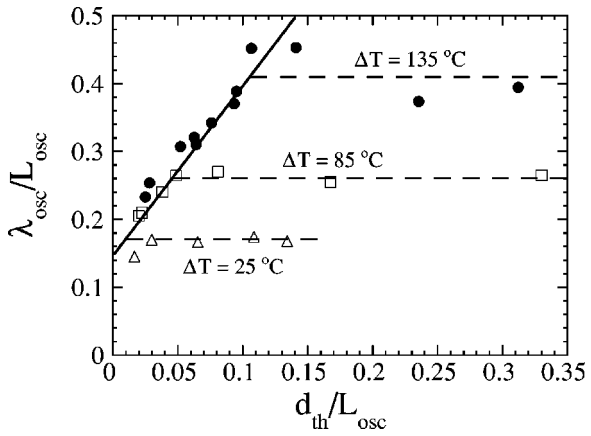

FIG. 16. Dimensionless oscillation wavelength λ_{osc}/L_{osc} at the instability threshold as a function of the dimensionless thermal diffusion length d_{th}/L_{osc} for different values of the temperature difference ΔT. Within the advective regime ($d_{th} < h$), all the values gather in a unique straight line, departing from this universal behavior in the low velocity diffusive regime ($d_{th} > h$). This shows that the scaling between the oscillation wavelength λ_{osc} and the oscillation threshold L_{osc} is completely controlled by the extension of the thermal gradient.

λ_{osc} with the driving velocity V for fixed values of ΔT and h, are drawn in Fig. 15. They manifest the same variation regimes with V as the critical distance L_c, meaning that they are related to the corresponding evolution of the thermal field through the distance h between the temperature baths at low velocities and the thermal diffusion length d_{th} at high velocities. In Fig. 16 we have reported the variations of the wavelength λ_{osc} with the thermal length d_{th}, both normalized in units of L_{osc}, for three values of the temperature difference ΔT between the two baths. The striking result is the gathering of all values λ_{osc}/L_{osc} in the thermal advection regime over a straight line, whatever the value of ΔT. This universal behavior clearly indicates that λ_{osc} is controlled by the thermal diffusion length d_{th}. When h controls the thermal field ($d_{th} > h$), λ_{osc}/L_{osc} deviates from this universal behavior, becoming velocity independent, confirming that the oscillation wavelength is controlled by the spatial extension of the temperature gradient.

Let us now focus on the mechanism of this oscillating instability. The stability of straight crack propagation is a fundamental problem of fracture mechanics but not yet well understood. It is related to the problem of the direction of propagation of a crack as a function of the external loading. In our case, straight propagation in the middle of the plate is, according to the symmetries, a pure mode I fracture problem. The fundamental question is: how a perturbation changes the stress field (apparition of shear stress, or mode II), and how the crack reacts to that new field. This requires a propagation condition in mixed-mode fracture (mode I + mode II). Crack initiation observations show that the presence of shear stress at the tip of the crack leads to a direction of growth making a finite angle with the initial crack direction. Assuming a generalization to growing cracks, this suggests that smooth propagation occurs along a path where the crack tip never feels shear stress, that is, $K_{II} = 0$. This is usually referred to as the criterion of local symmetry. Using this criterion, Cotterell and Rice [19] derived a stability condition for straight crack propagation, which states that straight crack growth becomes unstable when the nonsingular longitudinal tensile stress (called T in Ref. [19]) at the crack tip is positive. With such a stress, a perturbation of the direction of propagation will place the crack in an additional opening tensile stress, leading to an increase of the perturbation. This nonsingular component of the stress field has been computed from the elastic model using the measured thermal field, as done in Ref. [10] but using the measured thermal field, and the fracture energy Γ deduced from propagation thresholds. The Cotterell-Rice criterion predicts a destabilization of the straight crack much sooner ($L_{osc} \simeq 1.05 L_c$) than what is actually observed ($L_{osc} \simeq 1.7 L_c$) [7]. This discrepancy can be understood, recalling that this criterion considers straight propagation in an infinite medium. In our finite geometry, when escaping from straight path, the tip is no longer in the middle of the plate and should feel a stabilizing *geometric* shear stress, due to the rupture of symmetry.

Other models have been proposed to explain this instability. By means of finite element method, Bahr *et al.* [12] simulated the crack growth, using a discrete formulation of the criterion of local symmetry, i.e., at each time step, the crack direction is changed to suppress any shear stress at its tip. The main difference with the Cotterell-Rice analysis is the account for the finite width of the system. Because of the large computation time needed to achieve stationary state, they analyzed the stability of the straight crack growth by studying the relaxation of an oscillating crack towards its stationary state, through the time evolution of the oscillation's amplitude. The latter increases above the instability threshold, and decreases below. This analysis led to an instability threshold compatible with the experimental observations, though quantitative comparison cannot be performed as the used thermal field is only characterized by the thermal diffusion length d_{th}. On the other hand, the dependence of the oscillation wavelength agrees quantitatively with our measurement. They found a dependence of the wavelength λ_{osc} well fitted by $\lambda_{osc}/L_{osc} \simeq \alpha + \beta d_{th}/L_{osc}$ with $\alpha \simeq 0.14$ and $\beta \simeq 2.1$, to be compared with the experimental values of $\alpha \simeq 0.15$ and $\beta \simeq 2.5$ (Fig. 16). The oscillation wavelength λ_{osc} seems far less sensitive to the details of the thermal field than the critical widths L_c and L_{osc}, but is controlled by the spatial scale d_{th}.

A recent model, due to Adda-Bedia *et al.* [13] analyzes the bifurcation with an original stability criterion. Assuming a perturbation of the crack path as a sine function of a small amplitude, with the crack tip located in the middle of the plate, they calculate the resulting shear stress at the tip to first order in the amplitude. They state that the future evolution of the growth will tend to reduce that shear stress, leading either to an increase or a decrease of the perturbation. This different approach leads to results quantitatively similar to the preceding model [12], and confrontation with the experiment, by using the measured thermal field is under progress.

V. CONCLUSION

We have studied the quasistatic propagation of a directional crack. The straight propagation has been described through two characteristic quantities, the critical width L_c required for propagation, and the equilibrium crack tip position z_{tip}. These quantities enabled, by use of an elastic calculation of the energy release rate in the same thermal conditions, the extraction of the fracture energy Γ. We have shown that the apparent dependence of the fracture energy with the crack velocity V and the temperature difference ΔT could be understood as an effect of local temperature T_{tip} at the crack tip. This result is compatible with, through not directly comparable to, the effect of water vapor on surface energy of glass.

The stability of the straight crack propagation has been studied through the critical width L_{osc} and the oscillation wavelength λ_{osc}. Confrontation with recent theories shows that quantitative comparison requires the use of the real thermal field, because of the high sensitivity of the instability threshold L_{osc} to the details of the thermal field, though they recover the scaling of the wavelength λ_{osc} with the thermal diffusion length d_{th}. Here again, the systematic analysis of the dynamical characteristics of a system in the vicinity of the instability proves to be a powerful analysis tool as well as a fine test for the theory.

ACKNOWLEDGMENTS

We would like to thank F. Heslot, Y. Forterre, and J.Y. Bechler for fruitful discussions and helpful comments. The Laboratoire de Physique de la Matière Condensée is ''associé au Centre National de la Recherche Scientifique (CNRS), et aux Universités Paris 6 et Paris 7.''

[1] Y. Brecht and Z. Néda, Europhys. Lett. **32**, 475 (1995).
[2] A. Groisman and E. Kaplan, Europhys. Lett. **25**, 415 (1994).
[3] C. Allain and L. Limat, Phys. Rev. Lett. **74**, 2981 (1995).
[4] O. Ronsin and B. Perrin, Europhys. Lett. **36**, 435 (1997).
[5] E. Sharon, S.P. Gross, and J. Fineberg, Phys. Rev. Lett. **75**, 2117 (1996), and references therein.
[6] A. Yuse and M. Sano, Nature (London) **362**, 329 (1993).
[7] O. Ronsin, F. Heslot, and B. Perrin, Phys. Rev. Lett. **75**, 2352 (1995).
[8] J.F. Boudet, S. Ciliberto, and V. Steinberg, Europhys. Lett. **30**, 337 (1995).
[9] J.S. Langer, E.S.C. Ching, and H. Nakanishi, Phys. Rev. E **53**, 2864 (1996), and references therein.
[10] M. Marder, Phys. Rev. E **49**, R51 (1994).
[11] S. Sasa, K. Sekimoto, and H. Nakanishi, Phys. Rev. E **50**, R1733 (1994).
[12] H.A. Bahr, A. Gerbatsch, U. Bahr, and H.J. Weiss, Phys. Rev. E **52**, 240 (1995).
[13] M. Adda-Bedia and Y. Pomeau, Phys. Rev. E **52**, 4105 (1995).
[14] Sigmacote, Sigma-Aldrich Co.
[15] S.P. Timoshenko and J. N. Goodier, *Theory of Elasticity*, 3rd ed. (McGraw-Hill, New York, 1982).
[16] A.A. Griffith, Philos. Trans. R. Soc. London, Ser. A **221**, 163 (1920).
[17] B.R. Lawn and T.R. Wilshaw, *Fracture of Brittle Solids* (Cambridge University Press, Cambridge, 1975).
[18] T.A. Michalske and B.C. Bunker, J. Appl. Phys. **56**, 2686 (1984).
[19] B. Cotterell and J.R. Rice, Int. J. Fract. **16**, 155 (1980).